TITLE Post processing the U.S. National Water Model with a Long Short-Term Memory network

Jonathan M. Frame [1], Grey S. Nearing[1,2], Frederik Kratzert[3], Austin Raney [4] & Mashrekur Rahman [1]

[1]Department of Geological Sciences, University of Alabama; Tuscaloosa, AL USA
[2]Upstream Tech, Natel Energy Inc.; Alameda, CA USA
[3]LIT AI Lab & Institute for Machine Learning, Johannes Kepler University; Linz, Austria
[4]Department of Geography, University of Alabama; Tuscaloosa, AL USA

Abstract

The U.S. National Water Model (NWM) is a large scale hydrology simulator. Although NWM achieves coupling of multi-scale hydrological processes, its predictability at individual catchments can be improved. Hydrologic post-processing is an approach to reduce systematic simulation errors with statistical models, and has been shown to improve forecast accuracy of both calibrated and uncalibrated models. In this experiment we trained a Long Short-Term Memory (LSTM) network to post-process the NWM output, and tested performance at 531 basins across the continental United States. The LSTM post-processor provided a significant benefit to nearly all aspects of NWM streamflow predictions. The LSTM also benefited from NWM input - in particular, representation of hydrologic signatures improved, which indicates better representation of physical flow patterns.

---

1 Introduction

The U.S. National Water Model (NWM), based on WRF-Hydro (Cosgrove et al., 2015), is an emerging large scale hydrology simulator with 2.7 million river reaches. Some specific details of the NWM advancements in large scale hydrology are described by Elmer (2019, page 11), including increased resolution and number of stream reaches for a model covering this spatial domain. A strength of WRF-Hydro is simulating hydrologic dynamics (timing of the response) (Salas et al., 2018). The NWM is a useful tool in terms of hydrology over large spatial domains, but the performance has been shown to vary widely (Hansen, Shafiei Shiva, McDonald, & Nabors, 2019). Hansen et al. (2019) evaluated the performance of the NWM in the Colorado River Basin in terms of drought and low flows; they found better performance in the upper basin than the lower basin, and attributed the discrepancy to the NWM's success simulating snowpack hydrology. WRF-Hydro's performance at a regional scale show poor performance in the Southwest and Northern Plains (Salas et al., 2018). Sources of error in WRF-hydro may come from lakes, reservoirs, floodplain dynamics and soil parameter calibration (Salas et al., 2018).

The NWM version 2.0 is calibrated at 1,457 basins within the large scale domain of the Continental United States (CONUS). The USGS records daily streamflow at 28,529 sites[1]. Calibrating the model at each stream gauge within CONUS would be a prohibitively large computational expense. Regionalizing calibrated basins can be used to improve fore-

Corresponding author: Jonathan Frame, `jmframe@crimson.ua.edu`

[1] https://nwis.waterdata.usgs.gov/nwis

cast accuracy without having to calibrate each individual basin, but the accuracy in problematic regions would suffer (*e.g.*, Lower Colorado River and the Southwest). In the current stage of the NWM development the community should seek efficient and robust techniques to 1) make the best forecasts possible, and 2) maintain an agility and adaptability to future research which may continually increase forecast quality. There are promising results in the data science realm that may be directly (and immediately) applicable to the NWM.

Machine learning (ML) is gaining popularity in hydrological science, and there has been a call to merge ML with traditional hydrological modeling Reichstein et al. (2019). The Long Short-Term Memory network (LSTM) (Hochreiter, 1991; Hochreiter & Schmidhuber, 1997) is a time series deep learning method that is particularly well suited to model hydrologic processes (Kratzert, Klotz, Brenner, Schulz, & Herrnegger, 2018). LSTMs have been effective at simulating predictions of surface runoff at the daily time scale (Kratzert, Klotz, Shalev, et al., 2019), including in ungauged catchments where traditional methods of calibration do not work (Kratzert, Klotz, Herrnegger, et al., 2019). One potential problem with ML, however, is that it lacks a physical basis. While there are emerging efforts in hydrology to merge physical understanding with machine learning (e.g., Chadalawada, Herath, & Babovic, 2020; Daw et al., 2020; Pelissier, Frame, & Nearing, 2020; Tartakovsky, Marrero, Perdikaris, Tartakovsky, & Barajas-Solano, 2020), *theory informed machine learning* (Karpatne et al., 2017) is still relatively immature in hydrology.

Hydrologic post-processing is a straightforward theory-informed machine learning approach which avoids the problems of calibration across large spatial domains. This approach can remove sytematic errors in the model prediction, and has been shown to improve forecast accuracy of both calibrated and uncalibrated basins, particularly in wet basins (Ye, Duan, Yuan, Wood, & Schaake, 2014). The general methodology of post-processing involves taking the output of a process-based model and feeding it into a data-driven model. We suggest an immediate step for improving NWM forecast accuracy without the computational expense of calibration is post-processing streamflow predictions with ML. In this paper we apply a LSTM-based post processor for the NWM to improve basin-scale streamflow predictions.

The LSTM post-processor was applied to 531 basins across the CONUS. The basins chosen for this large scale analysis are mostly without engineered control structures, such as dams, canals, and levees. This was a deliberate choice made for the purpose of simulating a close-to-natural rainfall-runoff response. Our goal is to learn about basin-scale rainfall-runoff processes, rather than the hydraulic engineering implications resulting from simulated controlled flow, *e.g.* a reservoir release. Kim et al. (2020) show the limitation of the NWM to predict streamflow in a highly engineered watershed and the need for representing controlled releases. Thus we are using some of the simplest, and top performing, applications of the NWM for these experiments.

2 Methods

2.1 Data and models

2.1.1 Camels catchments

This study uses the Catchment Attributes and Meteorological dataset for Large Sample Studies (CAMELS) (CAMELS; Addor, Newman, Mizukami, & Clark, 2017; Newman et al., 2015). These data have been curated by the US National Center for Atmospheric Research(NCAR) [2]. We used 531 of the 671 basins - these were the same basins used by Newman et al. (2015), who excluded basins with large discrepancies in differ-

[2] https://ral.ucar.edu/solutions/products/camels

ent methods for measuring basin area and also basins larger than 2,000 km^2. CAMELS data include corresponding daily streamflow records from United States Geological Survey (USGS) gauges, and meteorological forcing data (precipitation, max/min temperature, vapor pressure and total solar radiation) come from North American Land Data Assimilation System (NLDAS; Xia et al., 2012).

2.1.2 National Water Model

We used the National Water Model version 2.0 reanalysis, which contains output from a 25-year retrospective simulation (January 1993 through December 2019)[3]. The NWM retrospective ingests rainfall and ingested other meteorological forcings from atmospheric reanalyses[4]. NWM output includes streamflow (point fluxes) and land surface (gridded) states and fluxes. The specific features that we used from the NWM output are shown in Table 1. To be compatible with the LSTM model, which uses a one-day timestep, we took the mean values across the calendar day (12AM - 11PM) to produce daily records from the hourly NWM output. Channel routing point data (CHRT) was collected at the NWM stream reach that corresponds to the stream gauge associated with each CAMELS catchment. Gridded land surface data (LDAS) was collected from each 1 km^2 Noah-MP cell contained within the boundaries of each CAMELS catchment, and these were averaged to produce a single representative (lumped) value for each catchment. Gridded routing data were similarly collected from each 250 m^2 cell, and we also included the maximum value within the catchment boundary. We did not include lake input and output fluxes because these would be inconsistent across basins (some basins have zero and some basins have multiple lakes). Note that the units of the NWM outputs are not required for the LSTM post-processor.

Table 1. National Water Model Output Data

Feature name	Feature	Resolution
ACCET	Accumulated evapotranspiration	1Km
FIRA	Total net long wave (LW) radiation to atmosphere	1Km
FSA	Total absorbed Short Wave (SW) radiation	1Km
FSNO	Snow cover fraction on the ground	1Km
HFX	Total sensible heat to the atmosphere	1Km
LH	Latent heat to the atmosphere	1Km
SNEQV	Snow water equivalent	1Km
SNOWH	Snow depth	1Km
SOIL M	Volumetric soil moisture	1Km
SOIL W	Liquid volumetric soil moisture	1Km
TRAD	Surface radiative temperature	1Km
UGDRNOFF	Accumulated underground runoff	1Km
streamflow	River Flow	point
q_lateral	Runoff into channel reach	point
velocity	River Velocity	point
qSfcLatRunoff	Runoff from terrain routing	point
qBucket	Flux from ground water bucket	point
qBtmVertRunoff	Runoff from bottom of soil to ground water bucket	point
sfcheadsubrt	Ponded water depth	250Km
zwattablrt	Water table depth	250Km

[3] https://docs.opendata.aws/nwm-archive/readme.html
[4] https://water.noaa.gov/about/nwm

2.2 Long Short-Term Memory network

The LSTM takes two types of inputs: daily meteorological forcings and static catchment attributes. Again, note that the units of the forcing data are irrelevant when used as inputs for the LSTM, which does not include a mass or energy balance. We used eighteen catchment attributes from the CAMELS dataset related to climate, vegetation, topography, geology, and soils. These are described in more detail by Addor et al. (2017) and listed in Table 2. Catchment attributes are static for each basin (do not change in time). We trained the LSTM with the the features described in Table 1 of Kratzert, Klotz, Herrnegger, et al. (2019). For a detailed explanation of the LSTM itself see (Kratzert et al., 2018).

For the post-processing runs we added the states, fluxes, and streamflow predictions from version 2.0 of the NWM. We trained the LSTM on water years 2004 through 2014 and tested the predictions on out-of-sample water years 1994 through 2002. The LSTM uses a 365-day LSTM look-back period, so a full year gap was left between training and testing to prevent bleedover (*i.e.* information exchange) between the two periods. We trained separate LSTMs with ten unique random seeds for initializing weights and biases, and calculated benchmarking statistics using the ensemble mean hydrograph. The LSTM makes predictions representing streamflow in units mm, reflecting an area normalized volume of water that moves through a stream at each model timestep. USGS gauge records (and the NWM predictions) are in units m^3/s. We used the geospatial fabric estimate of catchment area provided in the CAMELS dataset to convert all streamflow to units mm for our diagnostic comparison.

2.3 Experimental design

A simple schematic of the LSTM used as a post-processor for the NWM streamflow prediction is shown in Figure 1. The LSTM post-processor takes the NWM outputs as inputs, and the result is a LSTM-based streamflow prediction that is influenced by the process-based NWM.

As a quality check, we compared the results from each LSTM ensemble member, and found a relative standard error of the mean streamflow about 1%, and relative standard error of the NSE value of about 0.01%. This means that all LSTM solutions are similar between random initialization seeds. Gauch, Mai, and Lin (2019) attributed a 0.01 discrepancy in NSE values of the LSTM predictions to non-determinism of the loss function minimization. What Gauch et al. (2019) described as non-determinism exists as a result of the random seed, but running the training procedure twice with the same random seed gives an identical solution, satisfying the definition of determinism.

2.3.1 Performance metrics

We calculated a number of metrics for a robust evaluation of the predictive performance, including the NSE and KGE values (Ritter & Muñoz-Carpena, 2013). The variance, bias and Pearson correlation metrics were calculated separately as components of the NSE Gupta, Kling, Yilmaz, and Martinez (2009); these tell us about relative variability, mass conservation and linear correlation between the modeled/observed streamflow values, respectively. The metrics were calculated in two ways: 1) at each basin and then averaged together, and 2) using all of the flows from all basins combined.

Table 2. Table of LSTM Inputs

Meteorological Forcing Data	
Maximum Air Temp	2-meter daily maximum air temperature [$°C$]
Minimum Air Temp	2-meter daily minimum air temperature [$°C$]
Precipitation	Average daily precipitation [mm/day]
Radiation	Surface-incident solar radiation [W/m^2]
Vapor Pressure	Near-surface daily average [P_a]
Static Catchment Attributes	
Precipitation Mean	Mean daily precipitation
PET Mean	Mean daily potential evapotranspiration
Aridity Index	Ratio of Mean PET to Mean Precipitation
Snow Fraction	Fraction of precipitation falling on days with temp $< 0°C$
High Precipitation Frequency	Frequency of days with $\leq$ $5\times$ mean daily precipitation
Low Precip Frequency	Frequency of dry days (¡ 1 mm/day)
Elevation	Catchment mean elevation
Slope	Catchment mean slope.
Area	Catchment area
Forest Fraction	Fraction of catchment covered by forest
LAI Max	Maximum monthly mean of leaf area index
LAI Difference	Difference between the max. and min. mean of the leaf area index
GVF Max	Maximum monthly mean of green vegetation fraction
Soil Depth (Pelletier)	Depth to bedrock (maximum 50m).
Soil Depth (STATSGO)	Soil depth (maximum 1.5m).
Soil Porosity	Volumetric porosity.
Soil Conductivity	Saturated hydraulic conductivity.
Max Water Content	Maximum water content of the soil.
Sand Fraction	Fraction of sand in the soil.
Silt Fraction	Fraction of silt in the soil.
Clay Fraction	Fraction of clay in the soil.
Carbonate Rocks Fraction	Fraction of the catchment area characterized as 'carbonate sedimentary rocks'
Geological Permeability	Surface permeability (log10).

Our graphical results focus on three performance metrics: (i) Nash–Sutcliffe Efficiency measures the overall predictive performance as a correlation coefficient for the 1:1 linear fit between simulations and observations, (ii) Peak Timing Error measures the absolute value of differences (in units days) between simulated and observed peak flows for a given event, and (iii) Total Bias measures the overall bias of the simulated hydrograph relative to observations and represents how well the model matches the total volume of partitioned rainfall that passes through the stream gauge at each basin.

We also calculated performance metrics on different flow regimes. Rising limbs and falling limbs were characterized by a one-day derivative, where positive derivatives were categorized as rising limb, and negative derivatives as falling limb. High flows were characterized as all flow above the 80^{th} percentile in a given basin, and low flows as below the 20^{th} percentile in a given basin.

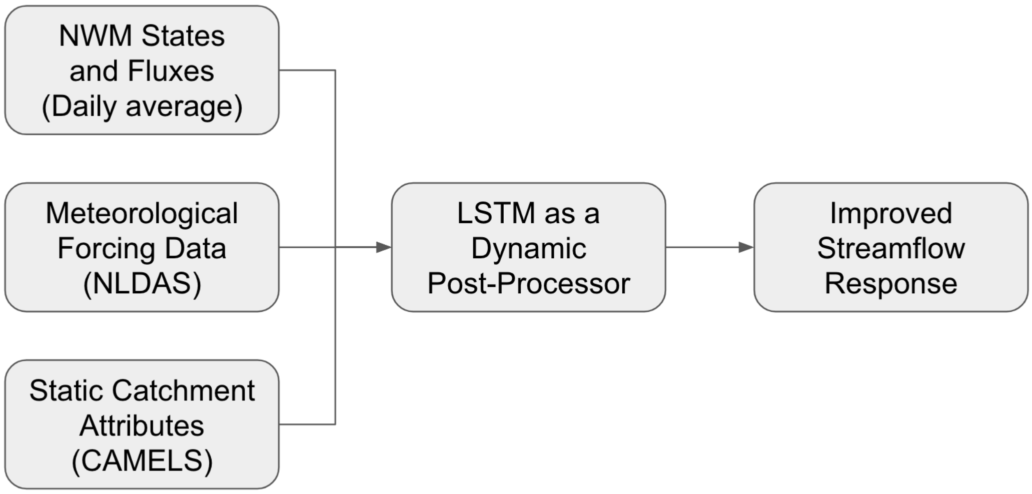

Figure 1. Flow chart showing the LSTM used as a post-processor for the NWM streamflow prediction.

We tested the performance of the LSTM post-procesor in different regions. We split the basins by USGS region[5], and averaged the NSE, bias and timing error of the CAMELS basins within each region.

We set an alpha value for statistical significance to $\alpha = 0.05$. To control for multiple comparisons we adjusted the alpha values using family-wise error rate equal to $1-(1-\alpha)^m$, with m being the number of significance tests (86), which brought our effective alpha value down to 0.049. We tested for statistical significance with a Wilcoxon signed-rank test against the null hypothesis that our test model (LSTM post-processor) performance across basins came from the same distribution as our base models (NWM and LSTM).

2.3.2 Simulated hydrograph representation of hydrologic signatures

Hydrologic signatures help us understand how well a model represents important aspects of real world streamflow, and where improvement should be made to the model's conceptualization Gupta, Wagener, and Liu (2008). We calculated the signatures listed in Table 2 of Addor et al. (2018) with model predicted values of streamflow. We calculated the true hydrologic signatures from USGS streamflow observations. The comparison between true values and predicted values was made with the correlation coefficient (r^2), higher values indicating better representation of hydrologic signature across basins by the model. We used the Steiger method to test for statistically significance improvement (or detriment) between the base models and the LSTM post-processor (Steiger & Browne, 1984).

2.3.3 Identifying basins best suited for post-processing with Random Forest regression

The LSTM post-processor did not improve performance at every basin. It is therefore valuable to know if the LSTM post-processor will work in any particular basin before implementation. We trained a random forest regression to predict the performance

[5] https://water.usgs.gov/GIS/regions.html

change between the LSTM and the LSTM post-processor at each individual basin. The inputs to the regression analysis were the performance score of the NWM streamflow predictions, hydrologic signatures and catchment characteristics. These regressors are useful to help interpret what basins might benefit most from the LSTM post-processor. We trained and tested random forests using k-fold cross-validation with 20 splits ($k = 20$) over the 531 basins. We report the correlation (r^2) of out-of-sample random forest predictions of post-processing improvements vs. real post-processing improvements. We also calculated the mean decrease in impurity (or Gini importance) to determine the total reduction of the criterion brought by each feature.

2.3.4 Interpretation of LSTM with integrated gradients

We calculated integrated gradients (Sundararajan, Taly, & Yan, 2017) to attribute the LSTM inputs (both atmospheric forcings and NWM outputs) to the total prediction of streamflow. Integrate gradients are a type of sensitivity analysis that are relatively insensitive to low gradients (e.g., at the extremes of neural network activation functions). Integrated gradients are calculated separately for each input, at each timestep, for each lookback timestep, in each basin. This means that for 9 years of test data with a 365-day lookback there are about 1.2 million integrated gradients per input, per basin.

2.3.5 Interpretation of LSTM with correlations between performance and NWM inputs

We made a direct connection between LSTM post-processor improvements with the NWM outputs using correlation. We calculated Pearson R values between the basin average value of each NWM input feature and the total performance change (NSE, bias and peak timing). These correlations were calculated for different flow regimes (all flows, rising/falling limbs, and high/low flows. The strengths of these correlations (positive or negative) indicate which types of basins (via NWM features) are benefiting most from the LSTM post-processor.

3 Results

3.1 Predictive performance

Post-processing the NWM with LSTMs significantly improved predictive performance. Figure 2 shows the cumulative distributions of three performance metrics (Nash–Sutcliffe Efficiency, Peak Timing Error , and Total Bias). Figure 2 also shows scatter plots comparing the performance of different models and includes r^2 values.

The LSTM post-processor improved the NSE score of the NWM mean daily streamflow at a total of 495 (93%) and reduces accuracy in 36 basins (7%) of the total 531 CAMELS basins. The LSTM post-processor improved the total bias of the NWM mean daily streamflow at a total of 331 (62%) of basins and the NWM mean daily streamflow at a total of 498 (94%) of basins. Improvements to performance in each basin are plotted spatially in Figure 3.

The LSTM post-processor improved predictions from the standalone LSTM in about half of the basins. The NSE score increased in a total of 299 (56%) and decreased in 232 basins (44%) of the 531 basins. Total bias improved in 258 (49%) of the basins. Peak timing improved in 234 (44%) and was a detriment in 222 (42%) of the basins. Performance improvements relative to the standalone LSTM are plotted spatially in Figure 4.

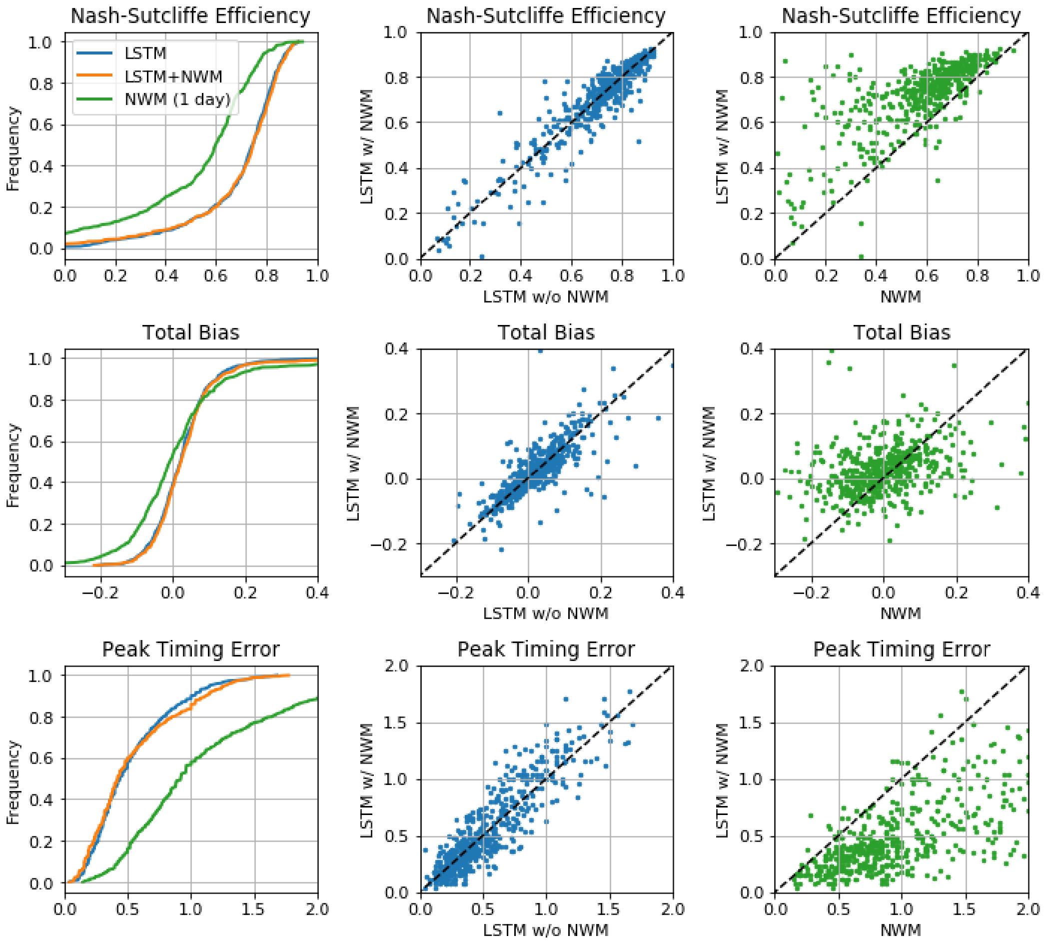

Figure 2. Results showing the cumulative distributions of model performance (Nash-Sutcliffe Efficiency, Total Bias and Peak Timing Error) over a 10-year test period in 531 CAMELS catchments. NWM is the National Water Model reanalysis averaged daily, LSTMs are Long Short Term Memory networks, and the LSTM w/ NWM represents the machine learning post-processed model with NWM inputs.

3.2 Performance by flow regime

The LSTM post-processor improved predictive performance of the NWM according to the NSE and KGE metrics, as well as their components (variance and correlation). A full set of performance metrics broken down by flow regime are shown in 4. The left side of the table shows the average of metrics calculated individually at each basin, and right side of the table shows the metrics as calculated combining the flows from all basins. The Nash-Suttcliffe Efficiency includes both mean and median averages, but the rest of the metrics are only averaged by median. Failure to reject the null hypothesis of significance (that the test model, LSTM post-processor, is different than the base models, NWM LSTM) is denoted by an asterisk.

In general this table shows that the performance of the LSTM post-processor is an improvement over the NWM in nearly all flow regimes, and by most metrics. The LSTM post-processor also improves upon the LSTM at a majority of the basins, and by most

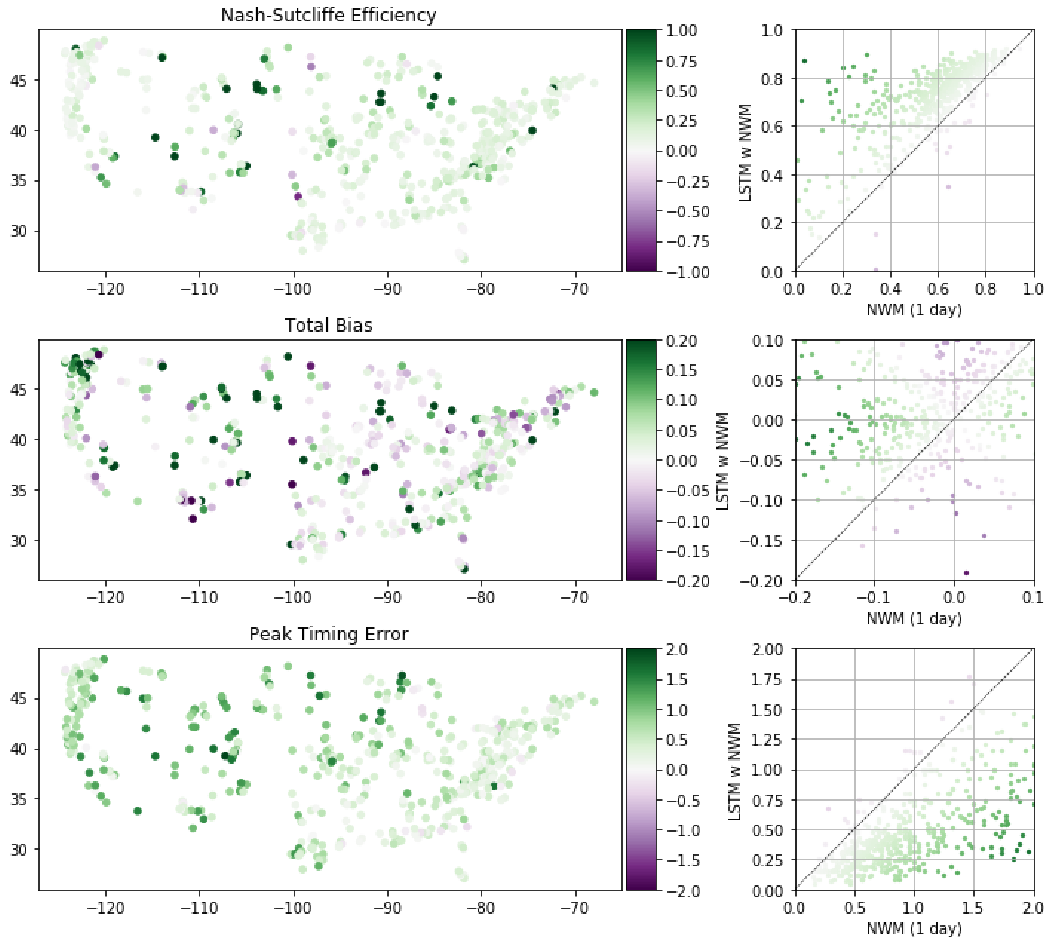

Figure 3. Improvements due to post-processing vs. the NWM in 531 CAMELS basins across CONUS. Green indicates basins where post-processing improved performance over the NWM (darker indicates larger relative improvement), and purple indicates basins where there was a decrease in performance (darker indicating worse relative detriment).

metrics. The rising limb and high flow regimes were improved by the LSTM post-processor according to every metric.

Bias is the only metric that was reduced due to post-processing, and the difference was highest in low flow regimes. Flows below the 20^{th} percentile are poorly predicted by all models. This is likely due to the fact that all models tend to have a difficulty predicting zero streamflow, and the 101 basins with periods of zero streamflow are weighing down the average. This will be discussed further in section 3.6 in terms of hydrologic signatures.

The right side of the table has better performance values than average of metrics calculated individually at each basin. This is a result of some of the better performing basins compensating for poorer performing basins, or from a different perspective, some basins have relatively poor performance which weighs down the average.

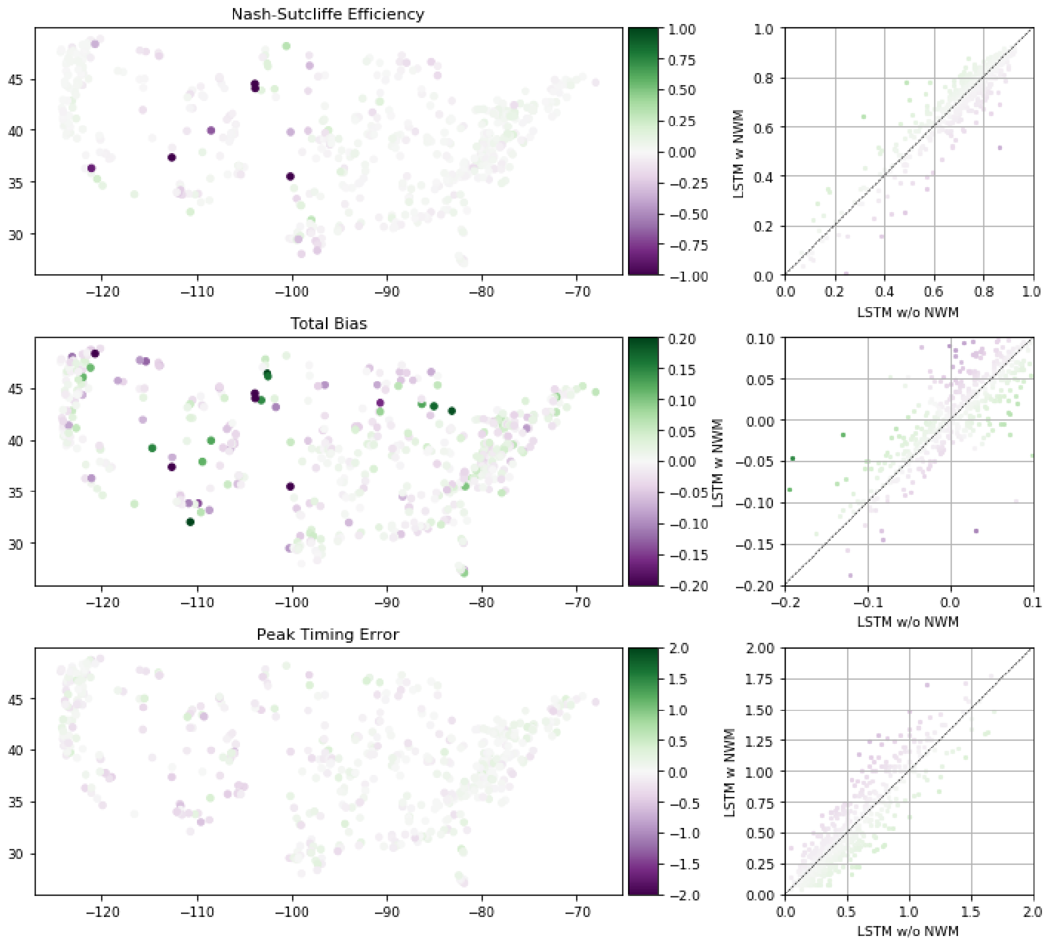

Figure 4. Improvements due to adding NWM states and fluxes as inputs into an LSTM in 531 CAMELS basins across CONUS. Green indicates basins where post-processing improved performance over the LSTM without NWM inputs (darker indicates larger relative improvement), and purple indicates basins where there was a decrease in performance (darker indicating worse relative detriment).

Table 3. Predictive performance for NWM, LSTM alone and the LSTM Post-processed NWM during various flow regimes.

Flow categories	Calculated Per-Basin						All Basins			
All flows	**NSE (mean)**	**NSE (median)**	**KGE**	**Variance**	**Bias**	**Pearson r**	**NSE**	**Variance**	**Bias**	**Pearson r**
NWM	0.44	0.60	0.64	0.83	-0.01	0.80	0.74	0.85	-0.02	0.86
LSTM	0.69	0.74	0.74	0.83	0.02	0.88	0.82	0.89	0.01	0.90
LSTM+NWM	0.67**	0.75	0.76	0.87	0.02	0.88**	0.82	0.93	0.02	0.91
Rising limbs	**NSE (mean)**	**NSE (median)**	**KGE**	**Variance**	**Bias**	**Pearson r**	**NSE**	**Variance**	**Bias**	**Pearson r**
NWM	0.46	0.58	0.55	0.73	-0.09	0.80	0.71	0.78	-0.07	0.85
LSTM	0.66	0.71	0.72	0.80	-0.01	0.86	0.78	0.85	-0.01	0.88
LSTM+NWM	0.65	0.72	0.74	0.85	0.00	0.87	0.79	0.89	-0.00	0.89
Falling limbs	**NSE (mean)**	**NSE (median)**	**KGE**	**Variance**	**Bias**	**Pearson r**	**NSE**	**Variance**	**Bias**	**Pearson r**
NWM	0.23	0.57	0.64	1.03	0.06	0.83	0.77	0.97	0.02	0.88
LSTM	0.69	0.78	0.77	0.92	0.05	0.90	0.87	0.96	0.03	0.93
LSTM+NWM	0.65**	0.77**	0.77**	0.94	0.05	0.90**	0.87	0.98	0.03	0.93
Above 80th percentile	**NSE (mean)**	**NSE (median)**	**KGE**	**Variance**	**Bias**	**Pearson r**	**NSE**	**Variance**	**Bias**	**Pearson r**
NWM	0.12	0.37	0.53	0.82	-0.12	0.70	0.67	0.83	-0.10	0.83
LSTM	0.53	0.58	0.67	0.81	-0.08	0.81	0.78	0.86	-0.06	0.88
LSTM+NWM	0.50**	0.60	0.69*	0.84	-0.07	0.81	0.79	0.90	-0.04	0.89
Below 20th percentile	**NSE (mean)**	**NSE (median)**	**KGE**	**Variance**	**Bias**	**Pearson r**	**NSE**	**Variance**	**Bias**	**Pearson r**
NWM	-18424.98	-16.64	-1.88	3.68	1.88	0.37	0.39	1.30	0.22	0.82
LSTM	-4749.68	-16.35	-1.31	2.85	3.27	0.43	0.56	1.26	0.33	0.89
LSTM+NWM	-5147.62	-14.66	-1.24	2.85*	2.87	0.43	0.58	1.28	0.30	0.90

Post-Processing Helps the NWM
Post-Processing Hurts the NWM
NWM Hurts the LSTM

* NWM post-processor is not significantly distinct from the NWM
** NWM post-processor is not significantly distinct from the LSTM

3.3 Performance by region

The LSTM post-processor significantly improves the NSE in fifteen of the eighteen regions. Note that region 9 is represented by only two CAMELS basins, which is not satisfactory for statistical evaluation. The bias was better represented by the NWM than the post-processor in five of the eighteen basins, including the entire East Coast (regions 1, 2 3), the Pacific Northwest (17) and the Lower-Colorado River (15). The timing was significantly improved at all regions with enough basins for a statistical evaluation.

Table 4. Predictive performance for NWM, LSTM alone and the LSTM Post-processed NWM in different regions.

		NSE		Bias		Timing	
Region	**n**	**NWM**	**LSTM + NWM**	**NWM**	**LSTM + NWM**	**NWM**	**LSTM + NWM**
1	22	0.60	0.78	-0.05	0.07	0.66	0.32
2	69	0.47	0.74	0.03	0.03	0.62	0.29
3	79	0.54	0.71	0.02	-0.02	0.78	0.49
4	30	0.42	0.69	0.00	0.05	1.13	0.64
5	35	0.61	0.74	-0.04	0.03	0.63	0.35
6	16	0.67	0.80	-0.01	0.00	0.73	0.24
7	29	0.43	0.71	0.11	0.09	1.17	0.50
8	7	0.61	0.67	0.01	-0.03	0.80	0.63
9	2	0.29	0.40	-0.16	0.09	2.52	1.29
10	49	-0.09	0.46	0.14	0.08	1.67	0.88
11	22	0.29	0.56	0.05	0.04	1.07	0.60
12	32	0.26	0.33	-0.01	-0.01	1.17	0.61
13	7	0.24	0.63	0.16	0.09	2.14	1.17
14	15	0.51	0.74	-0.03	0.01	2.12	1.01
15	14	-0.03	0.33	-0.02	0.12	1.56	0.94
16	5	0.22	0.71	-0.05	-0.03	1.82	0.89
17	72	0.66	0.81	-0.03	0.04	1.14	0.46
18	26	0.58	0.74	-0.03	0.00	1.35	0.58

Post-Processing significantly helps the NWM
Post-Processing significantly hurts the NWM

3.4 Random Forest regression

We assessed the LSTM post-processor's potential for improving predictions over the NWM at each individual basins. Figure 5 shows the results predicting the post processor improvement at each basins with an r^2 value of 0.82 between the true values and the predicted values. The strength of this prediction is heavily weighted by the outlier basins with abnormally large performance improvements from the post-processor. This means that the LSTM post-processor can improve the predictions in the basins where the NWM does most poorly.

Figure 5 also shows the (Gini) importance of each regression. The r^2 value was the same with all hydrologic signatures included in the regression as it was with only the four top importance-ranked signatures (full analysis not shown). This figure shows the results when only those four signatures were used. The baseflow index is the signature with the highest importance for predicting if the LSTM post-processor will be beneficial.

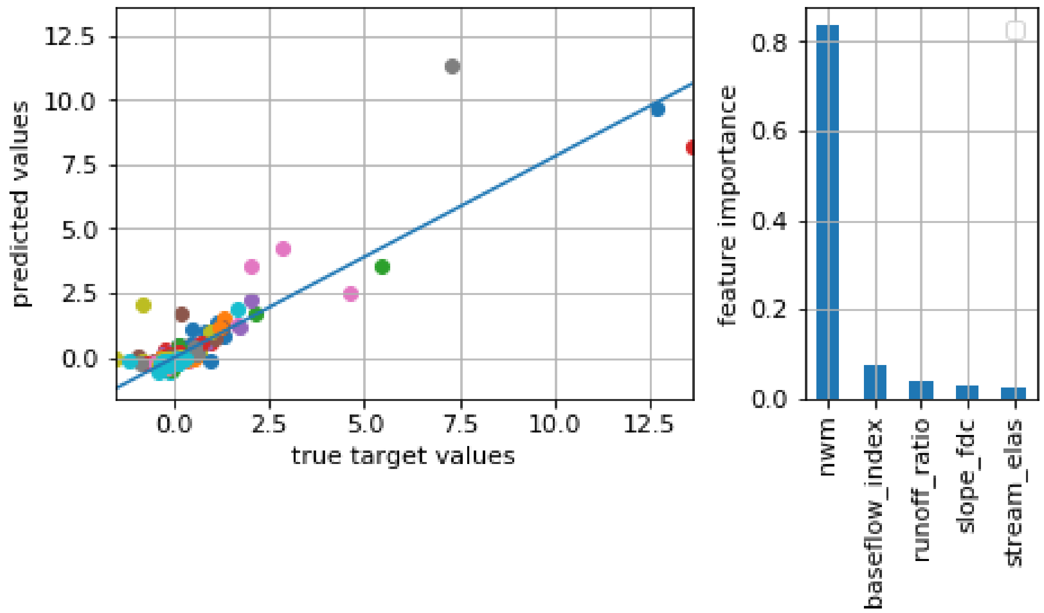

Figure 5. Predicting the LSTM post-processor improvement at each basin from with a random forest regression using NWM performance and hydrologic signatures as inputs. Left: Scatter plots for each of the 20 k-fold validation splits. Right: Average feature importance (across k-fold splits) on the prediction.

The aim of these results is understand whether it is possible to identify basins where post-processing might be beneficial. Although we found relatively high predictability in the improvement expected from post-processing, a problem is that we required knowing ahead of time the NWM performance to do so. This prevents us from predicting post-processing improvement in *ungauged* basins, since calculating the NWM performance requires streamflow observations. Without the NWM performance as a predictor in this regression we achieve a r^2 value of 0.37 using all the hydrologic signatures and all the static catchment attributes together. (Figure 6). A total of 45 catchment attributes and signatures were included as regression inputs, but the figure shows only the Gini importance of the top five. The baseflow index is again the most important signature for the regression, and the second signature being the slope of the flow duration curve. The basin area is the most important catchment characteristic, followed by the mean basin elevation.

3.5 Integrated gradients

Figure 7 shows the relative strength of the total attribution of the dynamic inputs to the LSTM post processor averaged across the entire validation period and across each basin. The ordered magnitudes of the integrated gradients can be interpreted as corresponding to the order of importance of inputs. The most important dynamic features for the LSTM post-processor were: (i) precipitation from NLDAS, and (ii) routed streamflow from the NWM point data. Precipitation inputs were weighted higher than the NWM streamflow output itself, which means that even when NWM streamflow data were available, the LSTM learned to get information directly from forcings rather then from the NWM streamflow output. This indicates that the LSTM post-processor generates a new rainfall-runoff relationship rather than relying on the NWM, which makes some sense

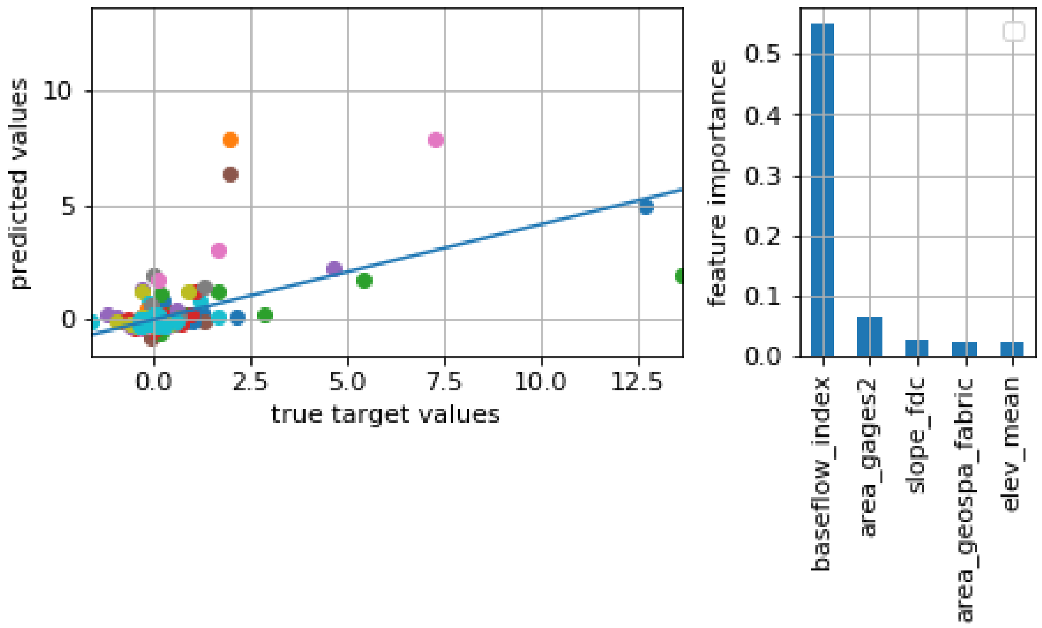

Figure 6. Predicting the LSTM post-processor improvement at each basin from with a random forest regression using static catchment attributes and hydrologic signatures as inputs. Left: Scatter plots for each of the 20 k-fold validation splits. Right: Top features ordered by Gini importance (averaged across k-fold splits) on the prediction.

given the overall results (Figure 2) that show similar performance between the LSTM with and without NWM inputs.

3.6 Correlations between NWM inputs and improvements

We need to show that the LSTM post-processor improves the predictions significantly in all regions, to address our comment in the introduction about the regional calibration being problematic in certain regions.

Figure 8 shows correlations (over 531 basins) between the time-averaged NWM inputs and changes in NSE scores of the LSTM post-processor relative to both the LSTM alone and NWM alone. These correlations were calculated using the whole hydrograph. Results for rising limbs and falling limbs of the hydrograph were qualitatively similar to this figure, and were therefore omitted. The rows of this figure show that correlation was weaker for differences in NSE score than Total Bias and Peak Timing Error. Performance differences between the NWM and the LSTM post-processor were most strongly (anti)correlated with stream velocity and underground runoff: basins with lower stream velocity (velocity) and less underground runoff (UGDRNOFF) saw greater performance improvement from (daily) post-processing. This means that in basins with high underground runoff and/or high stream velocity the LSTM post-processor improvements are smaller. In contrast, basins with higher total radiation (TRAD) and higher latent heat flux (LH) saw greater improvement due to post-processing. This means that in basins with more radiation and heat flux the LSTM post-processor improvements are larger. A direct interpretation of this could be that a flat meandering stream in the Southwest will benefit from the LSTM post-processor, which is consistent with the findings of (Salas et al., 2018). Performance differences between the LSTM alone and the LSTM post-processor were most strongly correlated with snow water equivalent and snow depth. This is con-

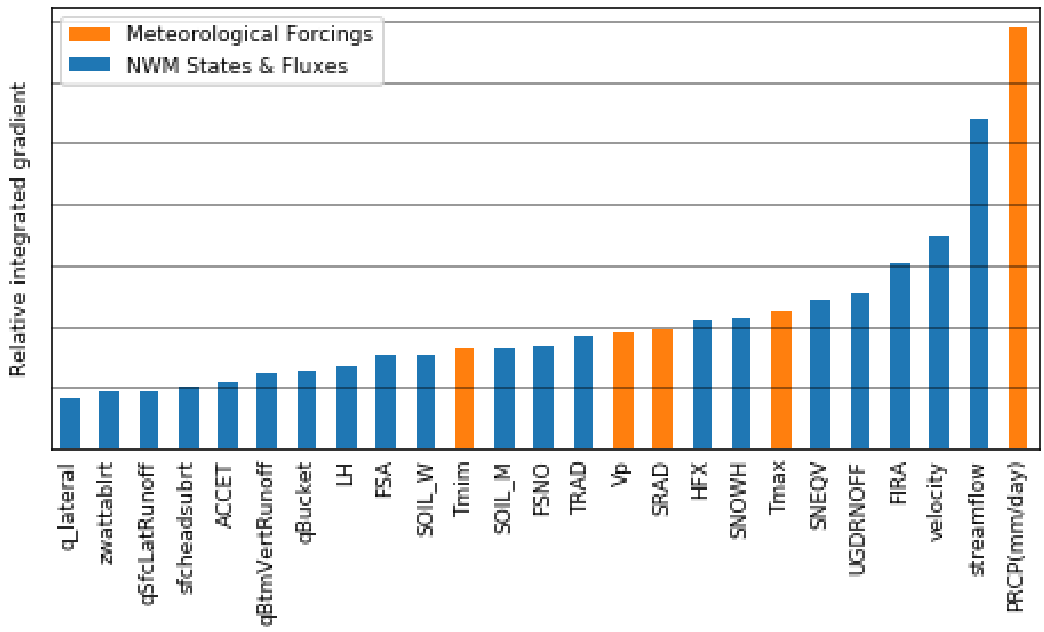

Figure 7. Attributions to the LSTM post-processor predictions. The vertical axis shows the relative magnitude of attribution (importance) for each input, with precipitation (PRCP) as the top contributor and NWM-predicted runoff into channel reach (q_lateral) contributing the least.

sistent with the findings of (Hansen et al., 2019) that the NWM represents snowpack hydrology well.

3.7 Representations of hydrologic signatures

Results of the analysis of hydrologic signature representation are shown in Figure 9, which also shows that the hydrologic signatures that at best represented by the NWM are similarly the best represented by the LSTM post-processor, and the same is true for the poorly represented hydrologic signatures. The overall r^2 values averaged across all signatures for the NWM, LSTM and LSTM post-processor were 0.59, 0.60 and 0.61, respectively.

The LSTM post-processor hurts the representation of the frequency of days with zero flow. There are 101 basins with any periods of zero flow. None of the models do well simulating zero flow, but the NWM is better at handling this situation, predicting zero flow periods at 56 basins. The LSTM and LSTM post-processor only predict periods of zero flows at 35 and 29 basins, respectively. This is an important characteristic in basins in the Southwest, where the NWM could use the benefit of the LSTM post-processor, so this would be a good place to focus future research of theory-guided ML for hydrology.

The LSTM post-processor makes a significant improvement over the NWM for several signatures. The improvement of runoff ratio, which is the fraction of precipitation that makes it through the stream gauge at the surface, could be a compensation for the uncalibrated soil parameters mentioned by (Salas et al., 2018). The improvement of mean half-flow date . The LSTM post-processor improves both high and low flow representations (5% 95% flow quantiles), which are important for natural resources management. The mean daily discharge is the best represented hydrologic signature by all models. This

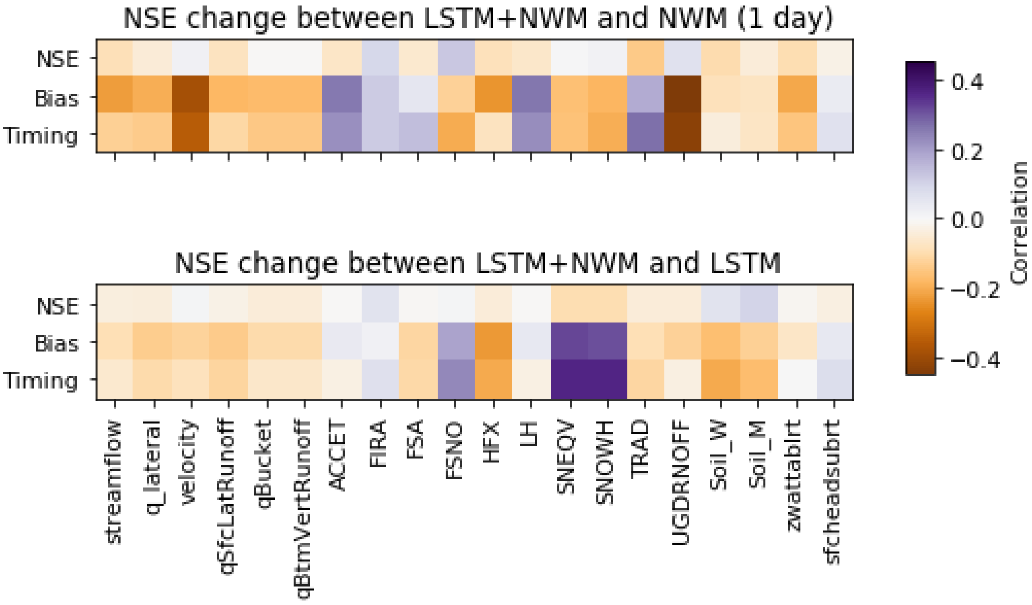

Figure 8. Correlations between the time-averaged NWM related inputs vs. NSE differences between the LSTM post-processor and both control models(LSTM alone and NWM alone).

is not surprising in terms of the LSTM and LSTM post-processor, because they were both trained to predict the mean daily discharge. It is also likely that the NWM calibrations, although not done at each basin, used mean daily discharge in the objective function.

The LSTM post-processor makes a significant improvement over the LSTM for baseflow index. This is the only signature which the LSTM post-processor improves both the NWM and the LSTM. This signature estimates the contribution of baseflow to the total discharge, which is computed by hydrograph separation. (Klemeš, 1986) (summarizing Lindsly's Applied Hydrology) cautions strongly against using hydrograph separation, because there is no real basis for distinguishing the source of flow in a stream. Even if the the baseflow index is only an coarse approximation of flow sources, the ability of the LSTM to improve on the representation, and even further by the LSTM post-processor, there is still some hydrologic conditions being represented.

4 Discussion

Results presented here show that the LSTM post-processor has potential to improve the daily averaged flow predictions of the NWM. The LSTM post-processor provided significant benefit to the NWM streamflow predictions at almost all (93%) of the 531 basins analyzed here. In the few basins where this was not the case, it may be possible to use fine tuning to calibrate a version of the post-processor that is specific to each gauge location (as would be done in traditional model calibration), however the LSTM post-processor used here can be applied to any basin, even ungauged. Right now, the post-processor is trained on naturalized basins, so further work would be needed to include reservoirs and other management practices. It is worth noting that the computational cost of training the LSTM post-processor is many orders of magnitude lower than parameter estimation in a distributed model like the NWM, and the computational cost of forward prediction is negligible. Both training and prediction over all 531 basins used here can be done on a laptop in a few hours, if necessary (we used a small GPU cluster).

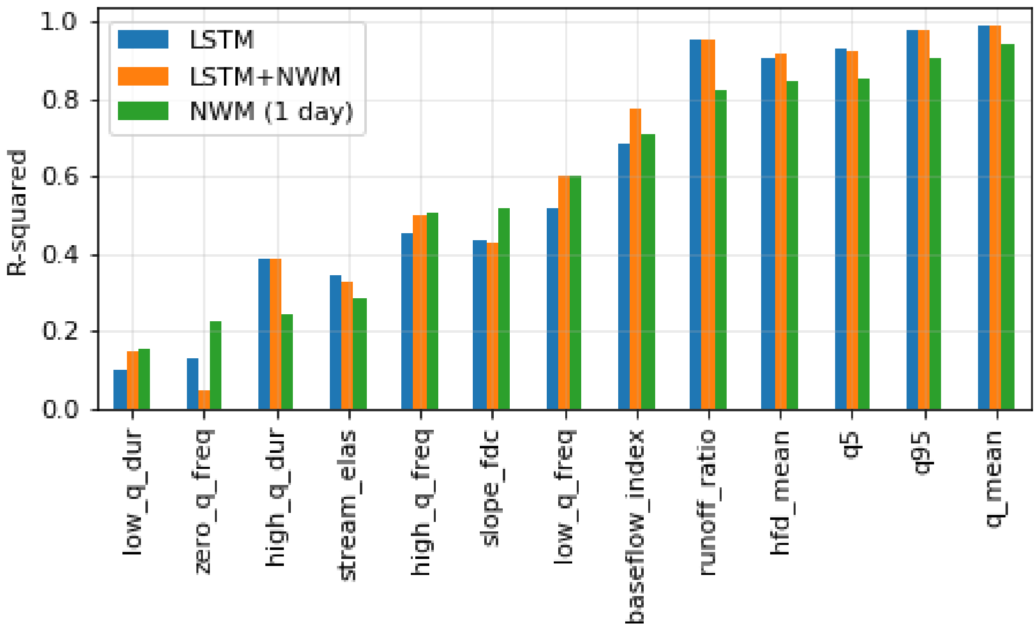

Figure 9. This plot shows the average representation of catchment hydrologic signatures by the NWM (blue), LSTM (orange) and the LSTM post-processor (green). The bars with the largest values represent the best performance.

The NWM performance and the performance improvement from the LSTM post-processor were negatively correlated: basins with low performance by the NWM have the highest performance change from the LSTM post-processor. This means that post-processing can be expected to correct situations where the NWM gives very bad predictions. Conversely, the performance of the NWM and the LSTM (without NWM inputs) were not correlated. Considering also that the overall performance of the LSTM changed only minimally from the addition of the NWM inputs and that the LSTM still preferred to extract more information from precipitation forcings, we might conclude that the LSTM post-processor learned a new representation of the rainfall-runoff response. The overall improvement in the representation of hydrologic signatures indicates this new rainfall-runoff response is a better representation of physical flow patterns than either the NWM or the LSTM. The interpretation of the integrated gradient and the correlations between improvement and NWM features indicate that this improvement of flow patters comes from information in the NWM representation of streamflow and snow states.

The NWM is not simply a rainfall-runoff simulator; it simulates flow through 2.7 million river reaches around CONUS, dam operations, land surface processes, hydraulics, and other complications of large domain hydrology. The nature of the CAMELS catchments selected in these experiments are such that they have few man made control structures, and are under 20,000 km^2. The results presented in this paper show that the LSTM post-processor improved streamflow predictions in similarly undisturbed catchments. Kratzert, Klotz, Herrnegger, et al. (2019) show that these predictions extend into ungauged basins. The immediate potential for improving real-time forecasting could be deploying this post-processor in undisturbed catchments, and undisturbed sub-catchments upstream of unnatural hydrologic conditions such as dams, agriculture lands and urban centers. An immediate next step would be to develop a post-processor that aggregates surface and subsurface runoff, but allows for the NWM router to aggregate these fluxes into streamflow.

This would allow for retaining conceptual representations of lakes and reservoirs that already exist in the NWM.

The post-processing procedure presented here is one of the more crude techniques currently available for combining process-based and data-driven models. Several other methods of combining the benefits of machine learning (predictability) with the benefits of physically realistic hydrologic theory (robustness) are in development. For example, (Pelissier et al., 2020) use Gaussian Processes to predict error between modeled and observed soil moisture, which allows ML to be used dynamically within a land surface model to correct the soil moisture state at each timestep of a simulation. Another example is using physical principals to constrain the loss function of an ML model during training. Implementing post-processing is relatively straightforward compared to other techniques such as adding physics into ML code, or using ML to dynamically updating the state variables.

Data Availability Statement:

All data and code used in this paper are publicly available in the following locations:

- U.S. National Water Model: `https://docs.opendata.aws/nwm-archive/readme.html`
- CAMELS data: `https://ral.ucar.edu/solutions/products/camels`
- Data processing code:`https://github.com/jmframe/nwm-reanalysis-model-data-processing`
- LSTM code: `https://github.com/kratzert/ealstm_regional_modeling`
- Post-processing and analysis code: `https://github.com/jmframe/nwm-post-processing-with-lstm`

Acknowledgments

Authors from the Johannes Kepler University were partially supported by a Google faculty research award. Jonathan Frame from the University of Alabama was partially supported by the NASA Terrestrial Hydrology Program. Grey Nearing from the University of Alabama was partially supported by the NCAR COMET program on a cooperative award with the National Water Center.

References

Addor, N., Nearing, G., Prieto, C., Newman, A. J., Le Vine, N., & Clark, M. P. (2018). A Ranking of Hydrological Signatures Based on Their Predictability in Space. *Water Resources Research*(i), 8792–8812. doi: 10.1029/2018WR022606

Addor, N., Newman, A. J., Mizukami, N., & Clark, M. P. (2017). The CAMELS data set: catchment attributes and meteorology for large-sample studies. *Earth Syst. Sci*, *21*, 5293–5313. Retrieved from `https://www.hydrol-earth-syst-sci.net/21/5293/2017/hess-21-5293-2017.pdf` doi: 10.5194/hess-21-5293-2017

Chadalawada, J., Herath, H. M., & Babovic, V. (2020). Hydrologically Informed Machine Learning for Rainfall-Runoff Modeling: A Genetic Programming-Based Toolkit for Automatic Model Induction. *Water Resources Research*, *56*(4), 1–23. doi: 10.1029/2019WR026933

Cosgrove, B., Gochis, D., Clark, E. P., Cui, Z., Dugger, A. L., Fall, G. M., ... others (2015). Hydrologic modeling at the national water center: Operational implementation of the wrf-hydro model to support national weather service hydrology. In *Agu fall meeting abstracts.*

Daw, A., Thomas, R. Q., Carey, C. C., Read, J. S., Appling, A. P., & Karpatne, A.

(2020). Physics-guided architecture (pga) of neural networks for quantifying uncertainty in lake temperature modeling. In *Proceedings of the 2020 siam international conference on data mining* (pp. 532–540).

Elmer, N. J. (2019). *Using Satellite Observations of River Height and Vegetation to Improve National Water Model Initialization and Streamflow Prediction* (Unpublished doctoral dissertation). The University of Alabama in Huntsville.

Gauch, M., Mai, J., & Lin, J. (2019). The Proper Care and Feeding of CAMELS: How Limited Training Data Affects Streamflow Prediction. , *2342*, 0–2. Retrieved from `http://arxiv.org/abs/1911.07249`

Gupta, H. V., Kling, H., Yilmaz, K. K., & Martinez, G. F. (2009). Decomposition of the mean squared error and NSE performance criteria: Implications for improving hydrological modelling. *Journal of Hydrology*, *377*(1-2), 80–91. Retrieved from `http://dx.doi.org/10.1016/j.jhydrol.2009.08.003` doi: 10.1016/j.jhydrol.2009.08.003

Gupta, H. V., Wagener, T., & Liu, Y. (2008). Reconciling theory with observations: elements of a diagnostic approach to model evaluation. *Hydrological Processes*, *2274*(November 2008), 2267–2274. doi: 10.1002/hyp.6989

Hansen, C., Shafiei Shiva, J., McDonald, S., & Nabors, A. (2019). Assessing Retrospective National Water Model Streamflow with Respect to Droughts and Low Flows in the Colorado River Basin. *Journal of the American Water Resources Association*, *55*(4), 964–975. doi: 10.1111/1752-1688.12784

Hochreiter, S. (1991). *Untersuchungen zu dynamischen neuronalen netzen* (Unpublished doctoral dissertation). Technische Universität München.

Hochreiter, S., & Schmidhuber, J. (1997). Long short-term memory. *Neural Computation*, *9*(8), 1735-1780. Retrieved from `https://doi.org/10.1162/neco.1997.9.8.1735` doi: 10.1162/neco.1997.9.8.1735

Karpatne, A., Atluri, G., Faghmous, J. H., Steinbach, M., Banerjee, A., Ganguly, A., … Kumar, V. (2017). Theory-guided data science: A new paradigm for scientific discovery from data. *IEEE Transactions on Knowledge and Data Engineering*, *29*(10), 2318–2331.

Kim, J., Read, L., Johnson, L. E., Gochis, D., Cifelli, R., & Han, H. (2020). An experiment on reservoir representation schemes to improve hydrologic prediction: coupling the National Water Model with the HEC-ResSim. *Hydrological Sciences Journal*, *0*(0), 1. Retrieved from `https://doi.org/10.1080/02626667.2020.1757677` doi: 10.1080/02626667.2020.1757677

Klemeš, V. (1986). Dilettantism in hydrology: Transition or destiny? *Water Resources Research*, *22*(9 S), 177S–188S. doi: 10.1029/WR022i09Sp0177S

Kratzert, F., Klotz, D., Brenner, C., Schulz, K., & Herrnegger, M. (2018). Rainfall-runoff modelling using long short-term memory (lstm) networks. *Hydrology and Earth System Sciences*, *22*(11), 6005–6022.

Kratzert, F., Klotz, D., Herrnegger, M., Sampson, A. K., Hochreiter, S., & Nearing, G. S. (2019). Towards Improved Predictions in Ungauged Basins: Exploiting the Power of Machine Learning. *Water Resources Research*, 2019WR026065. Retrieved from `https://onlinelibrary.wiley.com/doi/abs/10.1029/2019WR026065` doi: 10.1029/2019WR026065

Kratzert, F., Klotz, D., Shalev, G., Klambauer, G., Hochreiter, S., & Nearing, G. (2019). Towards learning universal, regional, and local hydrological behaviors via machine learning applied to large-sample datasets. *Hydrology and Earth System Sciences*, *23*(12), 5089–5110. doi: 10.5194/hess-23-5089-2019

Newman, A. J., Clark, M. P., Sampson, K., Wood, A., Hay, L. E., Bock, A., … Duan, Q. (2015). Development of a large-sample watershed-scale hydrometeorological data set for the contiguous USA: Data set characteristics and assessment of regional variability in hydrologic model performance. *Hydrology and Earth System Sciences*, *19*(1), 209–223. doi: 10.5194/hess-19-209-2015

Pelissier, C., Frame, J., & Nearing, G. (2020). Combining parametric land surface

models with machine learning. *arXiv preprint arXiv:2002.06141*.
Reichstein, M., Camps-valls, G., Stevens, B., Jung, M., Denzler, J., & Carvalhais, N. (2019). Deep learning and process understanding for data-driven Earth system science. *Nature*, *566*, 195 – 204. Retrieved from http://dx.doi.org/10.1038/s41586-019-0912-1 doi: 10.1038/s41586-019-0912-1
Ritter, A., & Muñoz-Carpena, R. (2013). Performance evaluation of hydrological models: Statistical significance for reducing subjectivity in goodness-of-fit assessments. *Journal of Hydrology*, *480*, 33–45. Retrieved from http://dx.doi.org/10.1016/j.jhydrol.2012.12.004 doi: 10.1016/j.jhydrol.2012.12.004
Salas, F. R., Somos-Valenzuela, M. A., Dugger, A., Maidment, D. R., Gochis, D. J., David, C. H., ... Noman, N. (2018). Towards real-time continental scale streamflow simulation in continuous and discrete space. *JAWRA Journal of the American Water Resources Association*, *54*(1), 7–27.
Steiger, J., & Browne, M. (1984). The comparison of interdependent correlations between optimal linear composites. *Psychometrika*, *49*(1), 11–24. doi: 10.1017/CBO9781107415324.004
Sundararajan, M., Taly, A., & Yan, Q. (2017). Axiomatic attribution for deep networks. *34th International Conference on Machine Learning, ICML 2017*, *7*, 5109–5118.
Tartakovsky, A. M., Marrero, C. O., Perdikaris, P., Tartakovsky, G. D., & Barajas-Solano, D. (2020). Physics-Informed Deep Neural Networks for Learning Parameters and Constitutive Relationships in Subsurface Flow Problems. *Water Resources Research*, *56*(5), 1–16. doi: 10.1029/2019WR026731
Xia, Y., Mitchell, K., Ek, M., Sheffield, J., Cosgrove, B., Wood, E., ... others (2012). Continental-scale water and energy flux analysis and validation for the north american land data assimilation system project phase 2 (nldas-2): 1. intercomparison and application of model products. *Journal of Geophysical Research: Atmospheres*, *117*(D3).
Ye, A., Duan, Q., Yuan, X., Wood, E. F., & Schaake, J. (2014). Hydrologic post-processing of MOPEX streamflow simulations. *JOURNAL OF HYDROLOGY*, *508*, 147–156. Retrieved from http://dx.doi.org/10.1016/j.jhydrol.2013.10.055 doi: 10.1016/j.jhydrol.2013.10.055